

Indication of a massive circumbinary planet orbiting the Low Mass X-ray Binary MXB 1658–298

Chetana Jain^{1*}, Biswajit Paul², Rahul Sharma³, Abdul Jaleel³ and Anjan Dutta³

¹*Hans Raj College, University of Delhi, Delhi 110007, India*

²*Raman Research Institute, Sadashivnagar, C. V. Raman Avenue, Bangalore 560080, India*

³*Department of Physics and Astrophysics, University of Delhi, Delhi 110007, India*

ABSTRACT

We present an X-ray timing analysis of the transient X-ray binary MXB 1658–298, using data obtained from the *RXTE* and *XMM – Newton* observatories. We have made 27 new mid eclipse time measurements from observations made during the two outbursts of the source. These new measurements have been combined with the previously known values to study long term changes in orbital period of the binary system. We have found that the mid-eclipse timing record of MXB 1658–298 is quite unusual. The long term evolution of mid-eclipse times indicates an overall orbital period decay with a time scale of $-6.5(7) \times 10^7$ year. Over and above this orbital period decay, the O-C residual curve also shows a periodic residual on shorter timescales. This sinusoidal variation has an amplitude of ~ 9 lt-sec and a period of ~ 760 d. This is indicative of presence of a third body around the compact X-ray binary. The mass and orbital radius of the third body are estimated to lie in the range, 20.5–26.9 Jupiter mass and 750–860 lt-sec, respectively. If true, then it will be the most massive circumbinary planet and also the smallest period binary known to host a planet.

Key words: X-rays: binaries: eclipsing, Stars: neutron, individual: MXB 1658–298, planet-star interaction

1 INTRODUCTION

Low Mass X-ray Binary (LMXB) systems consist of a compact object accreting from a low mass companion star. The orbit of the LMXBs is expected to evolve due to mass transfer and redistribution of the angular momentum arising from the interaction of the binary components.

The orbital evolution of X-ray binaries can be measured by four different ways. When the compact object is a pulsating neutron star, the pulse arrival time delay over the binary period is used to determine the orbital parameters of the system and multiple measurements of the orbital epoch over a long period are used to determine the orbital evolution (Levine et al. 2000). Orbital evolution in some black hole X-ray binaries (BHXBs), has been measured by constructing the radial velocity curve of the companion star from the doppler shifts of the spectral lines (González Hernández et al. 2014, 2017). In the eclipsing binaries, connecting the mid eclipse time can give information on the long term evolution of the orbital period and an accurate determination of orbital period derivatives (Wolff et al. 2009; Jain, Paul & Dutta 2010; Falanga et al.

2015; Islam & Paul 2016). The orbital evolution can also be measured from the stable orbital modulation of light curves (Chou & Grindlay 2001; Singh et al. 2002).

The orbital period of X-ray binaries can increase (for example, X 2127+119: Homer & Charles (1998); SAX J1808.4–3658: Jain, Dutta & Paul (2007); 4U 1822–37: Jain et al. (2010) 4U 1916–053: Hu, Chou & Chung (2008)) or decrease (for example, 4U 1820–30: Chou & Grindlay (2001); Her X-1: Paul et al. (2004), Staubert, Klochkov & Wilms (2009); A 0620–00 & XTE J1118+480: González Hernández et al. (2014); AX J1745.6–2901: Ponti et al. (2016); Nova Muscae 1991 González Hernández et al. (2017)) smoothly over several years of measurements. The orbital period can also undergo distinct epochs of sudden change, as observed in EXO 0748–676 (Wolff et al. 2009) and XTE J1710–281 (Jain & Paul 2011).

MXB 1658–298 is one of the rare LMXBs, that show X-ray eclipses in their light curves (Cominsky & Wood 1989). It is a transient X-ray source which was discovered in 1976 (Lewin, Hoffman & Doty 1976) from observations made with the SAS-3 X-ray observatory. Through several follow-up observations, an orbital period of ~ 7.1 hr and an eclipse duration of ~ 15 min were determined

* E-mail: chetana.jain11@gmail.com (CJ)

(Lewin et al. 1978; Cominsky & Wood 1984). About 2 years after its discovery, the X-ray intensity declined and the source was not detectable for the subsequent more than 20 years (in't Zand et al. 1999). During another outburst and a renewed activity in 1999, burst oscillations with a period of ~ 1.8 ms were reported (Wijnands, Strohmayer & Franco 2001), which could be the spin period of the neutron star. After being X-ray bright for about 2.5 years, the source went into quiescence near the beginning of 2001.

Comparing the orbital period of MXB 1658–298 measured from two eclipses during the first outburst and from four eclipses during the early part of the second outburst, Wachter, Smale & Bailyn (2000) reported an orbital period decay and determined an average decay timescale of 10^7 yr. But since this source was not detectable for a long time in between the two outbursts, there is no detailed record of the orbital period changes. Later, Oosterbroek et al. (2001) determined two more mid-eclipse times of MXB 1658–298, using the *Beppo-SAX* data during the second outburst. These measurements, along with the previous values, however, were not compatible with a simple orbital decay as was suggested earlier by Wachter et al. (2000). All the available eclipse measurements at this stage (eight), indicated some complexity in the orbital solution of this source.

Recently, MXB 1658–298 went into another outburst (Negoro et al. 2015), thus enabling a definitive study of its orbital evolution. In this work, we have determined mid-eclipse times using newer *RXTE*-PCA and *XMM-Newton* observations of this source, made during the second and the current outburst.

2 OBSERVATIONS AND ANALYSIS

The *RXTE*-PCA consists of an array of five collimated proportional counter units with a total photon collection area of 6500 cm^2 (Jahoda et al. 1996). We have analyzed 24 archived observations of MXB 1658–298 made with the *RXTE* observatory. The observation log is given in Table 1. The PCA data collected in the event mode was used to generate the light curves, using the `FTOOL-SEEXTRACT` from the astronomy software package `HEASOFT-ver 6.10`. The analysis was done in the energy band 2–20 keV. The background was estimated using the `FTOOL-PCBACKEST`. Faint source model was taken from the *RXTE* website. Thereafter, barycentric corrections were applied to all X-ray timings.

The *XMM-Newton* Observatory (Jansen et al. 2001) carries three X-ray mirrors and three focal plane instruments, each with a field of view of about $30' \times 30'$. Complete X-ray eclipses of MXB 1658–298 have been observed during two *XMM-Newton* observations. We have analyzed both of these archived observations. The first of these observations was made during the second outburst. It lasted for ~ 31.5 ks and covered two complete eclipses. Another ~ 42.9 ks long observation during the current outburst covered one complete eclipse. Observation details are summarized in Table 1. We have analyzed the 0.2–10 keV EPIC-PN data, using the XMM Science Analysis System (SAS version 8.0.0). Source counts were extracted from a circular region of radius $40''$ centered on the position of the target. Background events were extracted from a similar source-free circular region. Background subtracted light curves were barycenter

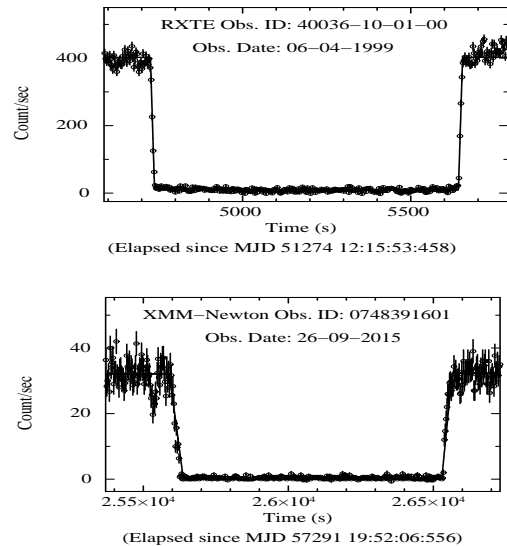


Figure 1. Sample of background subtracted light curves of MXB 1658–298 obtained from *RXTE*-PCA and *XMM-Newton* observations. The solid line in both the panels represents the best fit model as described in the text.

corrected using the SAS tool `BARYCEN`. Spectroscopic results from the February 2001 observation have been reported earlier by Sidoli et al. (2001). They have reported the presence of two eclipses. However, they did not report the mid-eclipse times for the purpose of orbital evolution measurement.

2.1 Eclipse Timing

Figure 1 shows two sample background subtracted light curves of MXB 1658–298, binned with 3 seconds and including an eclipse lasting for ~ 900 s. The mid eclipse times were determined by modeling each ingress and egress transition with a “step and ramp” model, which has been successfully employed in case of other eclipsing binaries (Wolff et al. 2009; Jain & Paul 2011). The variable parameters of the model are, the pre-ingress, eclipse, and post-egress count rates; the ingress and egress duration, the eclipse duration and the mid-eclipse time. Considering all the components to be freely variable, we first fitted the seven-parameter model to the light curves covering the eclipse and ~ 150 s before and after the eclipse (similar to Wolff et al. (2009)). For *RXTE*-PCA, it was found that the value of pre-ingress and the post egress count rates were similar and the eclipse ingress and egress duration were also similar within errors. The parameter space for *RXTE*-PCA, was thus reduced to five.

From all the observations of *RXTE* and *XMM-Newton*, we have determined 27 mid-eclipse time measurements. The mid-eclipse times and the corresponding 1σ statistical errors are given in Table 1. The durations of ingress and egress have been mentioned separately for the *XMM-Newton* observations. The orbit numbers are in accordance with the eclipse time measurements given in Wachter et al. (2000). As compared to other observations, the mid eclipse times determined from the *RXTE* observations have smaller error, except in two observations where count rate was relatively low.

Short timescale intrinsic variability in the intensity of the LMXB can modify the ingress/egress and thus effect the

mid-eclipse time measurements. Therefore, in order to estimate the additional random error in the mid-eclipse time measurements due to variability in the source, we simulated eclipses (with similar parameters as given in Table 1) at several positions in an *RXTE*-PCA light curve. Differences of the values of the mid-eclipse time that were used for simulation and those measured from the simulated data, were found to be about 1.3 seconds. Therefore, for further analysis, we have considered this value as an additional random error due to the intrinsic intensity variation of the LMXB, and have quadratically added it to the statistical error of each mid-eclipse time measurement.

2.2 Results

Since its discovery, MXB 1658–298 has undergone three outbursts. The first outburst lasted from 1976 to 1978, the second phase between 1999 - 2001; and the current phase of enhanced emission started around August 2015. Only two mid eclipse time measurements have been reported during the first active period. And during the current active phase of MXB 1658–298, so far we have only one measurement of the mid eclipse time. In contrast, from the second outburst, we have a total of 32 mid-eclipse time measurements with *RXTE*-PCA, *Beppo*-SAX and *XMM*-Newton.

We fitted a linear model to all the 35 mid eclipse time measurements. The best-fitting linear component was subtracted from the ephemeris history and the O-C residual curve is plotted in Figure 2. This curve hints at an orbital period decay in the system. It is also evident that over and above a secular orbital period decay, this source shows a periodic residual at a shorter timescale. The pattern of the residual can not be fitted with a higher order polynomial.

We fitted a model consisting of a quadratic and a sinusoidal function to the residual curve (Equation 1).

$$T_n = T_0 + nP_{orb} + \frac{1}{2}n^2P_{orb}\dot{P}_{orb} + A_{sin} \sin\left(\frac{2\pi(n-n_0)}{P_{sin}}\right) \quad (1)$$

In this equation, P_{orb} is the orbital period at epoch T_0 . The parameters, A_{sin} , P_{sin} and n_0 are the amplitude, period and phase of the sinusoidal function, respectively. The best fit parameters are given in Table 2 and the best fit model is shown in Figure 2, after subtracting the best fit linear model. The timescale for evolution of the orbital period ($\tau = P_{orb}/\dot{P}_{orb}$) is $6.5(7) \times 10^7$ yr. It is larger than an earlier estimate using fewer mid-eclipse times (Wachter et al. 2000) by a factor of ~ 6 . The sinusoidal variation in the O-C curve could be due to light travel time delay for motion of the X-ray binary in the presence of a third body.

3 DISCUSSION

We have determined 27 new mid-eclipse times of the X-ray binary MXB 1658–298 using data from *RXTE* and *XMM*-Newton observatories. These measurements have been used to determine the orbital evolution in this system.

Orbital evolution of LMXBs is complex and is known to display different trends. The orbital separation is known to increase in most of the LMXBs, at timescales which are shorter than that predicted by a conservative mass transfer or by gravitational wave radiation (Homer & Charles

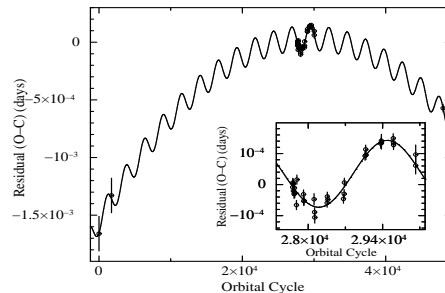


Figure 2. The mid-eclipse times of MXB 1658–298 and the best fit model are shown here after subtracting a linear fit to the data. The inset figure shows enlarged view of the residuals during the second outburst.

1998; Hartman et al. 2009). A decreasing orbital period has been observed in a few LMXBs and some short period BHXBs. But the orbital decay in these systems is also unusual and is much faster than that predicted by conventional methods of gravitational wave radiation, magnetic braking and mass loss from the system (González Hernández et al. 2014; Ponti et al. 2016). Interaction with a third body could be responsible for a large orbital decay observed in two LMXBs (Peuten et al. 2014; Iaria et al. 2015). Orbital period glitches have been observed in a couple of LMXBs, and are attributed to be due to magnetic cycling of the secondary star (Wolff et al. 2009; Jain & Paul 2011). Even though most of the LMXBs show a reasonably good quadratic fit to the mid-eclipse time records, there are signatures of deviation from a constant orbital period derivative present on longer timescales (Iaria et al. 2015; Chou et al. 2016; Patruño et al. 2016).

The mid-eclipse time history of MXB 1658–298 seems to be quite unusual. The combined data spanning three outbursts and covering ~ 40 years of timeline, indicates an orbital decay. In addition, a large number of measurements in a two year period during the second outburst show sinusoidal variation in the eclipse timing residual, perhaps indicating the presence of a third body around this source.

We can consider the X-ray binary (the inner binary) to be a point mass in an approximate binary motion with this third body. In that case, the sinusoidal residual is due to orbital motion of the inner binary around the center of mass of the whole system. This is similar to the pulse arrival time delay of a binary X-ray pulsar, except that instead of a periodic pulse, we have a periodic eclipse.

For a $1.4 M_{\odot}$ neutron star, the mass of the companion star lies between 0.25 – $0.9 M_{\odot}$ (Cominsky & Wood 1984). Assuming the radius of the orbit of the X-ray binary (having an estimated total mass in the range 1.65 – $2.3 M_{\odot}$) around the center of mass of the system to be same as amplitude of the sinusoidal residual, the third body (assumed to be co-planar with the inner binary) should have a mass range of 0.0195 – $0.0257 M_{\odot}$ (i.e., 20.5 – 26.9 Jupiter mass) and an estimated range for orbital radius between 750 – 860 lt-sec.

The two extremes of this estimation are graphically shown in Figure 3. Taking M_b and R_b as the mass and radius of orbit of the binary; and M_{tb} and R_{tb} as the mass and orbital radius of the third object, we have drawn curves for the expressions below for two extremes of the mass of the inner binary, i.e., $1.65 M_{\odot}$ (dashed line) and $2.3 M_{\odot}$ (solid

Table 1. Measurements of the mid-eclipse times of MXB 1658–298.

Observation Date	Instrument/ Mission	Observation ID	Orbital Cycle	Mid eclipse time MJD (d) ^{a, b}	Duration of Eclipse (sec) ^a	Duration of Ingress/Egress (sec) ^a
1976-10-07	SAS-3	–	0	43058.72595 (15) ^c	–	–
1978-03-07	HEAO-1	–	1740	43574.64413 (15) ^c	–	–
1999-04-05	RXTE	40414-01-01-00	27707	51273.9780792 (15) ^d	–	–
1999-04-06	RXTE	40036-10-01-00	27709	51274.5711027 (37)	903.10 (15)	12.78 (12)
1999-04-09	RXTE	40414-01-02-00	27720	51277.8326259 (37) ^d	–	–
1999-04-10	RXTE	40050-04-02-00	27722	51278.4256585 (41)	909.69 (15)	10.65 (5)
1999-04-13	RXTE	40414-01-03-00	27733	51281.6871743 (37) ^d	–	–
1999-04-15	RXTE	40414-01-04-00	27740	51283.7627259 (32) ^d	–	–
1999-04-17	RXTE	40050-04-07-00	27747	51285.8382399 (21)	899.24 (15)	9.97 (20)
1999-04-26	RXTE	40050-04-15-00	27778	51295.0298420 (58)	905.50 (15)	9.788 (3)
1999-04-29	RXTE	40050-04-16-00	27787	51297.6984644 (58)	908.24 (15)	10.51 (4)
1999-06-05	RXTE	40414-01-05-00	27911	51334.4649765 (23)	898.51 (25)	8.55 (50)
1999-06-06	RXTE	40414-01-06-00	27915	51335.6509729 (35)	894.23 (20)	16.72 (56)
1999-06-08	RXTE	40414-01-07-00	27920	51337.1334964 (42)	898.72 (15)	10.69 (34)
1999-08-03	RXTE	40414-01-09-00	28110	51393.4693583 (116)	902.10 (80)	11.09 (32)
1999-08-06	RXTE	40414-01-10-00	28119	51396.1378573 (41)	898.76 (65)	12.42 (45)
1999-08-07	RXTE	40414-01-11-00	28123	51397.3238583 (122)	895.85 (70)	11.26 (38)
1999-10-15	RXTE	40414-01-12-00	28355	51466.1129515 (23)	904.77 (25)	9.78 (46)
1999-10-16	RXTE	40414-01-14-00	28359	51467.2989903 (23)	901.70 (15)	13.49 (31)
1999-10-18	RXTE	40414-01-13-00	28368	51469.9675212 (23)	898.99 (25)	16.04 (42)
2000-01-14	RXTE	40414-01-15-00	28663	51557.4363538 (29)	904.40 (20)	12.32 (31)
2000-01-18	RXTE	40414-01-16-00	28676	51561.2909286 (12)	909.02 (15)	9.48 (32)
2000-01-19	RXTE	40414-01-17-00	28680	51562.4769833 (23)	902.36 (35)	14.67 (53)
2000-05-13	RXTE	50410-01-01-00	29069	51677.8173235 (23)	901.50 (25)	16.26 (36)
2000-05-17	RXTE	50410-01-02-00	29082	51681.6719031 (17)	906.41 (15)	12.18 (23)
2000-05-18	RXTE	50410-01-03-00	29086	51682.8579030 (58)	902.26 (20)	13.59 (64)
2000-08-08	RXTE	50410-01-06-00	29363	51764.9896893 (58)	905.13 (20)	11.68 (48)
2000-08-12	Beppo-SAX	–	29376	51768.844257 (16) ^e	–	–
2000-08-13	Beppo-SAX	–	29378	51769.437259 (15) ^e	–	–
2000-10-18	RXTE	50410-01-07-00	29600	51835.2612753 (58)	909.21 (15)	11.15 (44)
2000-10-19	RXTE	50410-01-08-00	29604	51836.4472795 (51)	907.53 (10)	10.34 (15)
2000-10-20	RXTE	50410-01-09-00	29606	51837.0402811 (58)	906.15 (15)	11.34 (35)
2001-02-20	XMM-Newton	0008620701	30022	51960.386091 (23)	903.13 (50)	15 (2)/ 15.5 (5)
2001-02-20	XMM-Newton	0008620701	30023	51960.682631 (28)	902.75 (84)	19 (1)/ 19.2 (1)
2015-09-26	XMM-Newton	0748391601	48004	57292.129569 (32)	900.95 (40)	47 (3)/ 22 (4)

^a Number in brackets give the 1σ statistical error.^b An independent random error due to intrinsic source variability has been added quadratically for further analysis.^c These numbers are taken from Cominsky & Wood (1989)^d These numbers are taken from Wachter et al. (2000)^e These numbers are taken from Oosterbroek et al. (2001)**Table 2.** Orbital ephemerides of MXB 1658–298

Parameter	Best fit value ^a
T_0 (MJD)	43058.72606 (23)
P_{orb} (d)	0.296504619 (11)
\dot{P}_{orb}	$-1.25 (13) \times 10^{-11}$
A_{sin} (lt-sec)	9.20 (75)
P_{sin} (d)	764 (37)
n_0	28846 (28)
χ^2 (d.o.f)	46.65 (29)

^a The numbers in bracket indicate the 1σ errorsline), respectively. (Here, G is the gravitational constant.)

$$R_{tb} = \frac{M_b R_b}{M_{tb}}; R_{tb} = \left(\frac{GP_{sin}^2}{4\pi^2} \right)^{1/3} \frac{M_b}{(M_b + M_{tb})^{2/3}} \quad (2)$$

In Figure 3, the square markers indicate these estimated parameters for two extremes of the mass of the inner binary. Depending on the mass of the inner binary, the true mass and orbital radius of the third body will lie on the dotted line connecting these square markers. The additional errors in these two parameters due to the uncertainty in period and amplitude of the sinusoidal component have been estimated by a Monte Carlo simulation. The additional 1σ uncertainty is represented by two dash-dotted lines parallel to the diagonal (dotted) line.

The mass and orbital radius of the third body have been estimated assuming a circular and co-planar orbit. There is no evidence of circularity except that the residual shown in Figure 2 is consistent with being sinusoidal. Co-planarity is

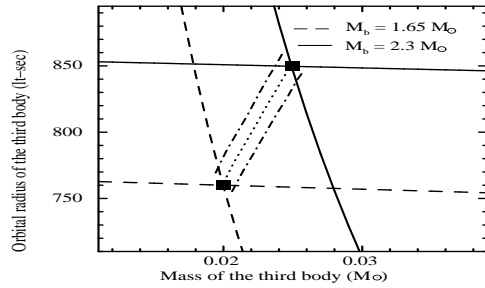


Figure 3. Graphical representation of finding the mass and orbital radius of the third body. The square shaped markers indicate the mass and orbital radius of the third body for a binary mass of $1.65M_{\odot}$ (dashed line) and $2.3M_{\odot}$ (solid line), respectively.

a reasonable assumption as the circumbinary planets discovered with Kepler are nearly co-planar (Welsh et al. 2014)

Though rarer compared to planets around single stars, about 20 circumbinary planets are known among ~ 1000 eclipsing binaries observed with Kepler (Welsh et al. 2014). If true, the third body in the present system is the most massive circumbinary planet; exceeding Kepler-1647b by a factor of about 15 (Kostov et al. 2016). Simulations of planet formation and migration around binary stars show the most stable planets to be in the sub-Saturn mass range while more than Jupiter mass planets, if present, are likely to have large orbits around the binary (Pierens & Nelson 2008).

The binary period of MXB 1658-298 is also much shorter compared to the orbital period of all the binary stellar systems around which planets have been found, the shortest binary period being 7.4 days in Kepler-47 (Orosz et al. 2012). The lack of planets around short period binaries is believed to be related to the process of angular momentum loss that brings the two stars closer in the process of binary evolution (Welsh et al. 2014).

The system MXB 1658-298 gives important new input for the range of stellar configurations for which circumbinary planets may form and survive migration over several stages of binary evolution. In particular, the binary system being a low mass X-ray binary and having an age of several billion years is an important input for the study of planet formation and migration around binary stellar systems.

ACKNOWLEDGMENTS

This research has made use of data obtained from the High Energy Astrophysics Science Archive Research Center, provided by NASA’s Goddard Space Flight Center. The authors thank S. Sridhar for insightful discussions.

REFERENCES

Chou Y., Grindlay J. E., 2001, *ApJ*, 563, 934
 Chou Y., Hsieh H.-E., Hu C.-P., Yang T.-C., Su Y.-H., 2016, *ApJ*, 831, 29
 Cominsky L. R., Wood K. S., 1984, *ApJ*, 283, 765
 Cominsky L. R., Wood K. S. 1989, *ApJ*, 337, 485
 Falanga M., Bozzo E., Lutovinov A., Bonnet-Bidaud J. M., Fetisova Y., Puls J., 2015, *A&A*, 577, 130

González Hernández J. I., Rebolo R., Casares J., 2014, *MNRAS*, 438, L21
 González Hernández J. I., Suárez-Andres L., Rebolo R., Casares J., 2017, *MNRAS*, 465, L15
 Hartman J. M., Patruno A., Chakrabarty D., Markwardt C. B., Morgan E. H., van der Klis M., Wijnands R., 2009, *ApJ*, 702, 1673
 Homer L., Charles P. A., 1998, *New Astron.*, 3, 435
 Hu C.-P., Chou Y., Chung Y. Y., 2008, *ApJ*, 680, 1405
 Iaria R., Di Salvo T., Gambino A. F., Del Santo M., Romano P., Matranga M., Galiano C. G., Scarano F., Riggio A., Sanna A., et al., 2015, *A&A*, 582, 32
 int Zand J., Heise J., Smith M. J. S., Cocchi M., Natalucci L., Celidonio G., 1999, *IAUC*, 7138
 Islam N., Paul B., 2016, *MNRAS*, 461, 816
 Jahoda K., Swank J. H., Giles A. B., Stark M. J., Strohmayer T., Zhang W., Morgan E. H., 1996, *SPIE*, 2808, 59
 Jain C., Dutta A., Paul B., 2007, *JAA*, 28, 197
 Jain C., Paul B., Dutta A., 2010, *MNRAS*, 409, 755
 Jain C., Paul B., 2011, *MNRAS*, 413, 2
 Jansen F. et al., 2001, *A&A*, 365, L1
 Kostov V. B., Orosz J. A., Welsh W. F., Doyle L. R., Fabrycky D. C., Haghighipour N., Quarles B., Short D. R., Cochran W. D., Endl M., et al., 2016, *ApJ*, 827, 86
 Levine A. M., Rappaport S. A., Zojcheski G. 2000, *ApJ*, 541, 194
 Lewin W. H. G., Hoffmann J. A., Doty J., 1976, *IAU Circ.*, 2994
 Lewin W. H. G., Marshall H., Primini F., Wheaton W., Cominsky L., Jernigan G., Ossman W., 1978, *IAUC*, 3190
 Negoro H., Furuya K., Ueno S., Tomida H., Nakahira S., Kimura M., Ishikawa M., Nakagawa Y. E., Mihara T., Sugizaki M., et al., 2015, *ATel*, 7943, 1
 Oosterbroek T., Parmar A. N., Sidoli L., in’t Zand J. J. M., Heise J., 2001, *A&A*, 376, 532
 Orosz J. A., Welsh W. F., Carter J. A., Fabrycky D. C., Cochran W. D., Endl M., Ford E. B., Haghighipour N., MacQueen P. J., Mazeh T., et al., 2012, *Science*, 337, 1511
 Patruno A., Jaodand A., Kuiper L., et al., 2016 *arXiv* 1611.06023
 Paul B., Naik S., Bhatt N., 2004, *Nuclear Physics B Proc. Suppl.*, 132, 548
 Peuten M., Brockamp M., Kupper A. H. W., Kroupa P., 2014, *ApJ*, 795, 116
 Pierens A., Nelson R. P., 2008, *A&A*, 483, 633
 Ponti G., De K., Munoz-Darias T., Stella L., Nandra K., 2017, *MNRAS*, 464, 840
 Sidoli L., Oosterbroek T., Parmar A. N., Lumb D., Erd C., 2001, *A&A*, 379, 540
 Staubert R., Klochkov D., Wilms J., 2009, *A&A*, 500, 883
 Singh N. S., Naik S., Paul B., Agrawal P. C., Rao A. R., Singh K. Y., 2002, *A&A*, 392, 161
 Wachter S., Smale A. P., Baily C., 2000, *ApJ*, 534, 367
 Welsh W. F., Orosz J. A., Carter J. A., Fabrycky D. C., 2014, in *IAU Symposium*, 293, 125
 Wijnands R., Strohmayer T., Franco L. M., 2001, *ApJ*, 549, L71
 Wolff M. T., Ray P. S., Wood K. S., Hertz P. L., 2009, *ApJS*, 183, 156